

Article

Exploring the Detection of Cl⁻ Penetration in Portland Cement Mortars via Surface Electrical Resistivity

Miguel Alberto Pablo-Calderón , Prisciliano Felipe de Jesús Cano-Barrita *  and Frank Manuel León-Martínez 

CIIDIR Unidad Oaxaca, Instituto Politécnico Nacional, Calle Hornos No. 1003, Colonia Noche Buena, Sta. Cruz Xoxocotlán, Oaxaca 71230, Mexico; mpabloc1600@alumno.ipn.mx (M.A.P.-C.); fmleonm@ipn.mx (F.M.L.-M.)

* Correspondence: pcano@ipn.mx

Abstract: Surface electrical resistivity is a non-destructive technique that is sensitive to the microstructure of hydrated cement paste and the chemical composition of the pore solution in cement-based materials. In this study, a Wenner array was used to measure changes in mortar resistivity due to chloride ion diffusion as a function of electrode separation. Specimens were made from four mortar mixtures: 100% Ordinary Portland cement and 60% cement + 40% fly ash at two water/binder ratios of 0.55 and 0.40. The specimens were subjected to unidirectional chloride ion diffusion in a 2.8 M NaCl solution for 175 days. To determine the chloride penetration depth, three methods were used: silver nitrate spraying, chloride concentration profiles via potentiometric titration, and chloride concentration profiles via inversion of the resistivity data using the RES1D software (version 1.00.09 Beta). The results showed a linear relationship between the chloride ion penetration depth obtained via inversion of the surface electrical resistivity data versus the penetration depth from colorimetry and from chloride concentration profiling (both with $R^2 = 0.8612$). Chloride penetration changed the conductivity of the pore solution; therefore, the resistivity decreased when increasing both the chloride concentration and the penetration depth. Inversion of surface resistivity data obtained with a Wenner array permitted non-destructive determination of chloride penetration. However, these results were obtained under laboratory environmental conditions and other scenarios must be addressed for wider applications.

Keywords: pozzolanic reaction; hydration; chloride diffusion; Friedel's salt; pore solution



Citation: Pablo-Calderón, M.A.; Cano-Barrita, P.F.d.J.; León-Martínez, F.M. Exploring the Detection of Cl⁻ Penetration in Portland Cement Mortars via Surface Electrical Resistivity. *Materials* **2023**, *16*, 7123. <https://doi.org/10.3390/ma16227123>

Academic Editors: Grzegorz Peruń and Tangbin Xia

Received: 27 September 2023
Revised: 2 November 2023
Accepted: 4 November 2023
Published: 10 November 2023



Copyright: © 2023 by the authors. Licensee MDPI, Basel, Switzerland. This article is an open access article distributed under the terms and conditions of the Creative Commons Attribution (CC BY) license (<https://creativecommons.org/licenses/by/4.0/>).

1. Introduction

The durability of concrete structures is affected by chloride ion ingress, which can corrode the reinforcing steel bars. Chloride ions may enter cement-based materials through mixing with water or by external sources from environmental exposure [1]. Chlorides from external sources are mainly transported into the concrete through diffusion, which is influenced by factors like porosity, pore size distribution, ion exchange, and the chemical/physical binding of chlorides into the C-S-H and AFm phases. The capacity of chloride binding in hardened cement paste is affected by the C₃A and C₄AF content in cement, pore solution composition, addition of supplementary cementitious materials (SCMs), and leaching that alters the hydrate composition [2,3]. Chemical binding leads to the formation of Friedel's salt, which removes chlorides from the pore solution [4]. The mechanisms of ingress and the binding of chlorides in cement systems are complex, as several processes are acting simultaneously. Porosity in cement-based materials is directly related to their mechanical properties and permeability. High porosity and a well-connected pore network facilitate the ingress of harmful species that cause the deterioration of reinforced concrete structures. Porosity and pore size distribution may be estimated using mercury intrusion porosimetry [5] or nuclear magnetic resonance relaxometry [6].

There are different standard techniques used to determine the ability of concrete to resist chloride ion ingress. One technique is the rapid chloride permeability test (RCPT) [7],

which measures the amount of electrical charge passing through a saturated cylindrical concrete sample (100 mm in diameter and 50 mm in thickness) when a potential difference of 60 V of direct current is applied for six hours. This test has been subject to criticism, although it has been adopted as a standard and is widely used. The main drawbacks are that the current passed through the specimen is related to all ions in the pore solution; the measurements are made before steady-state migration is achieved; and the high voltage applied leads to an increase in temperature, which further increases the charge passed through. Another similar test is the non-steady-state migration test NT BUILD 492 [8]. This test applies an electrical potential to force chloride migration through the specimen, and the penetration depth is measured by spraying a silver nitrate solution on the fractured surface. A non-steady-state migration coefficient is then calculated. The AASHTO T 259 [9] is another type of test that measures the resistance of hardened concrete to chloride penetration by ponding the surface of concrete slabs with a three percent NaCl solution for 90 days. There is difficulty in interpreting the results because the specimens are subject to diffusion and wicking effects. Two additional tests, NT BUILD 443 [10] and ASTM C1556 [11], measure the accelerated penetration of chlorides in hardened concrete for the determination of the apparent diffusion coefficient and surface concentration based on chloride concentration profiles. These tests are expensive and time-consuming.

The techniques mentioned previously are destructive, which limits them to one measurement per test, and their results may show high variability [12]. On the other hand, there are non-destructive tests, such as ASTM C1876 [13] and AASHTO TP119 [14], that determine the bulk electrical resistivity or bulk conductivity of concrete. While these tests require molded specimens or specimens cored from actual structures, the surface electrical resistivity test on saturated concrete samples can indirectly assess the permeability of the material and provide an indication of its resistance to chloride ion penetration [15]. The Wenner array method is one test used for concrete electrical resistivity measurements that utilize four equally spaced surface electrodes. It is non-destructive [16], easy to use, rapid, and can be conducted on the same sample without special preparation [17]. According to Oleiwi et al. [18] and Cosoli et al. [16], the Wenner technique is one of the most widely used techniques for in situ tests on the surface of concrete. However, currently, there are still no widely accepted standards, other than AASHTO T358 [19], for measuring the surface electrical resistivity using the Wenner four-electrode method. Factors affecting resistivity measurements include porosity; pore size and connectivity; the tortuosity of the pore network and the composition of the pore solution, which are determined by the type of cementitious material; and the water/binder ratio (w/b). The curing method and sample conditioning also affect resistivity because they influence the properties of the pore solution, the degree of saturation, and temperature. Ambient temperature and relative humidity can be the most difficult conditions to control in real-life applications [20]. The accuracy of resistivity measurements is also dependent on the quality of the contact between the electrodes and the concrete surface. To create an electrolytic contact between the electrodes and the concrete surface, different solutions can be used. These include saturated sponges, soaked wooden plugs, a conductive gel, or localized wetting. However, these methods do not improve the contact between the electrodes and the concrete surface to a significant extent [20]. Studies indicate that the best resistivity measurements are obtained using the Wenner configuration with the largest electrode spacing [21]. An increase in separation will result in a greater penetration of the current field, covering more volume that results in lower relative values. In addition, resistivity measurements are substantially wrong if the semi-infinite geometry assumption is not met in small concrete specimens.

Regarding concrete resistivity and chloride penetration, there is an inverse correlation between resistivity and the chloride diffusion rate [22]. In addition, resistivity may be used to classify the risk of corrosion of a specific concrete structure, with low resistivities corresponding to a high risk of corrosion and vice versa. Qiao et al. [23] related the electrical resistivity of air-entrained concrete to the formation factor of the material. They found that increasing the air content decreased the formation factor of saturated concrete due to a

higher volume of fluid-filled air voids. As w/c increased, the formation factor decreased due to a higher porosity and connectivity. Other uses of resistivity include the estimation of the chloride diffusion coefficient that may be required for the service life estimation of reinforced concrete structures [24]. Higher resistivities correspond to lower chloride diffusion coefficients. The only study identified in the literature related to the present study was that of Fares et al. [25], who inverted electrical resistivity tomography (ERT) data to obtain resistivity profiles as a function of depth. They used a Wenner configuration with 14 electrodes, two concrete mixtures, and a mortar exposed to chloride diffusion. The chloride profiles obtained via ERT were compared with those obtained using the chloride content of powder samples. They observed a good agreement between ERT and destructive testing.

The purpose of this study was to investigate the feasibility of determining the chloride ion penetration depth in mortar specimens under laboratory conditions by inverting surface resistivity data obtained with a commercial Wenner array instrument with variable electrode spacing. The resistivity measurements were performed as a function of time. The estimated chloride depth was compared with the penetration depth obtained from the colorimetric test using a 0.1 N AgNO₃ solution sprayed on a freshly broken surface, as well as from chloride content profiles at a depth where the concentration was approximately zero. The relationship between the depths obtained non-destructively and those obtained using standard destructive tests will be explored.

2. Materials and Method

2.1. Materials

Ordinary Portland cement (OPC), class F fly ash (FA), and river sand were used. The relative density of the sand was 2.66 g/cm³, with an absorption of 2.81% [26] and a fineness modulus of 3.28. The chemical composition of the cementitious materials used is shown in Table 1. The river sand grading is provided in Figure 1.

Table 1. Chemical composition (% by mass) of the cementitious materials used [27].

Main Oxides	SiO ₂	Al ₂ O ₃	Fe ₂ O ₃	CaO	TiO ₂	P ₂ O ₅	MgO	Na ₂ O	K ₂ O	SO ₃	LOI
OPC	21.07	3.69	4.50	61.93	0.97	0.10	1.83	0.09	0.30	2.54	4.38
FA	62.28	20.38	4.09	4.68	0.94	0.38	0.98	0.31	0.99	-	3.43

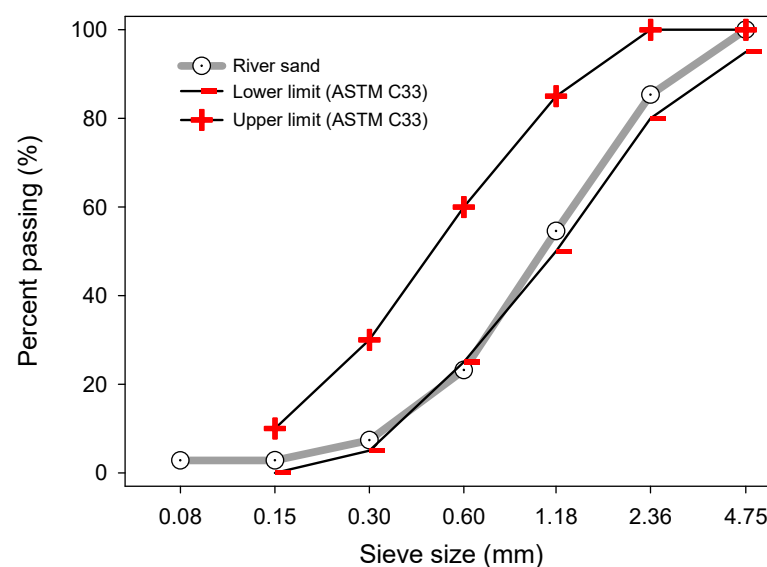


Figure 1. River sand grading used to prepare the mortar mixes.

2.2. Method

2.2.1. Preparation and Conditioning of Mortar Specimens

Mortar mixes with water/binder (w/b) ratios of 0.55 and 0.40 and a sand/binder (s/b) ratio of 2.75 were prepared according to the procedure described in the ASTM C192 standard [28]. Table 2 provides the mortar mixture proportions. The sand/binder ratio (s/b) of 2.75 was used as proposed in ASTM C109 [29] for preparing the Portland cement mortars. The w/b ratios were selected as 0.55 and 0.40 in order to produce relatively high and low chloride ion diffusion coefficients and low and high electrical resistivities. Two mortars used 100% OPC and the other two used 60% OPC + 40% FA, by mass, which were labeled as OPC0.55, FA0.55, OPC0.40, and FA0.40, respectively. FA was included in the mixes because it significantly reduces the porosity and pore size distribution in hardened cement paste, which, in turn, reduces the electrical resistivity of concrete. In addition, cement pastes containing FA chemically bind a higher amount of chlorides compared with plain OPC cement pastes. A total of 18 mortar specimens were cast from each mortar mix. Table 3 provides details on the shape and dimensions of the different specimens. As is shown in Figure 2, the size of the prismatic mortar specimens was determined to minimize edge effects and to consider the space as semi-infinite, taking the value of a as less than $1/3$ of the thickness of the specimens (approximately $a = h/3$) [21,30,31]. Parameters α and β are dependent on the electrode spacing. The former represents the distance from the center of the electrode to the edge of the prism and it is perpendicular to the electrode array; β is the distance from the external electrode to the edge of the prism and it is parallel to the electrode array. Therefore, the dimensions were 25 cm in width, 40 cm in length, and 15 cm in height. A geometric correction factor of approximately 1.0 was obtained from the specimen size to minimize edge effects in the surface electrical resistivity measurements [21,31].

Table 2. Mortar mixture proportions.

Material (kg)	Mix			
	OPC0.55	FA0.55	OPC0.40	FA0.40
Cement	518	301	562	326
Fly ash	-	200	-	217
Sand	1425	1381	1544	1493
Water	285	276	225	217

Table 3. Characteristics of mortar specimens prepared from each mix.

Test	Type	Dimensions				Quantity
		w (cm)	l (cm)	h (cm)	Ø (cm)	
Surface electrical resistivity	Control prisms	25	40	15	10	2
	* Prisms	25	40	15		2
	Control cylinders		20			4
Colorimetry/chloride content profiles	Control cubes	15	15	15		2
	* Cubes	15	15	15		8

* Specimens for measurements at 7, 28, 112, and 175 days of exposure to chloride ion diffusion.

The specimens were cured via immersion in a calcium-hydroxide-saturated solution for 28 and 220 days. The longest curing time was chosen to reduce the effect of hydration reactions on the resistivity measurements. Control specimens remained in the curing conditions throughout the experiment. After the curing period, a marine epoxy coating was applied to the surface of the prismatic and cubic specimens, leaving one face of the prisms (25 cm × 40 cm) and one face of the cubes without any epoxy coating. By leaving the epoxy-coating-free faces in a 2.8 M sodium chloride solution, according to the NT BUILD 443 standard [10], the specimens were exposed to unidirectional chloride ion diffusion for 7, 28, 112, and 175 days before testing. The control specimens were kept in a saturated calcium

hydroxide solution. As an accelerated test, NT BUILD 443, requires a NaCl concentration that is approximately 5 times the concentration found in seawater.

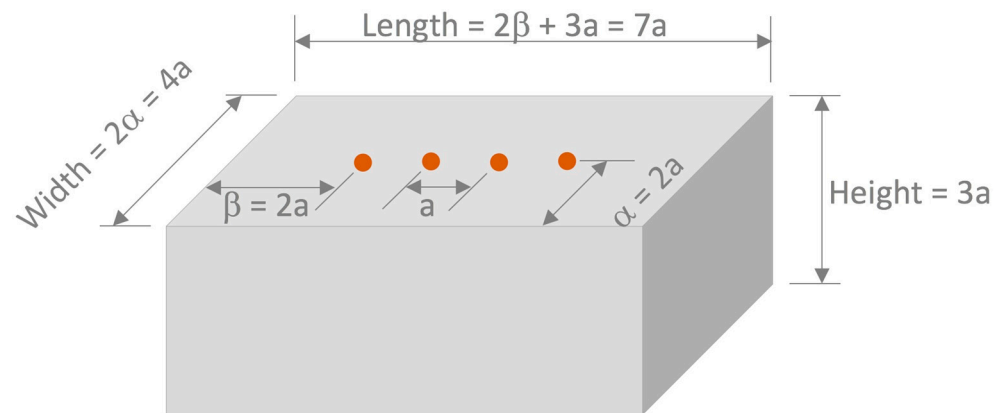


Figure 2. Criteria for estimating minimum specimen dimensions to minimize edge effects in surface electrical resistivity (r) measurements (geometric correction factor of approximately 1, and a represents the electrode spacing) [21,31].

2.2.2. Surface Electrical Resistivity Measurements

The surface electrical resistivity was measured using a Resipod resistivity meter (Proceq, Schwerzenbach, Zurich, Switzerland) with a Wenner array and a geometric fixture with variable electrode separation (Figure 3). There are four electrodes in the Wenner array: two external and two internal. External electrodes (A and B) apply an alternating current, while the internal electrodes (M and N) measure the potential difference. To avoid edge effects and, consequently, an overestimation of the resistivity values, the prism size was calculated according to the recommendations provided by Gowers and Millard [31] and Chun-Tao Chen et al. [32]. The resistivity readings were taken at the center along the longitudinal direction of the sample. Two axes perpendicular to each other, one longitudinal and the other transverse, were sketched on the surface of the specimens (Figure 4). The separations between the electrodes a were 3.8, 4.0, 4.2, 4.4, and 4.6 cm. The resistivity tests were performed on the saturated, surface-dry specimens under laboratory conditions at approximately 23 ± 1 °C. Four test groups were studied, two of which were prismatic specimens with 28 and 220 days of curing and were exposed to different chloride diffusion times. The third group had chloride-free prismatic and cylindrical specimens with 28 days of curing and $a = 38$ mm. Finally, the fourth had prismatic and cylindrical specimens with 220 days of moist curing and were exposed to different chloride diffusion times and using a value of $a = 38$ mm.

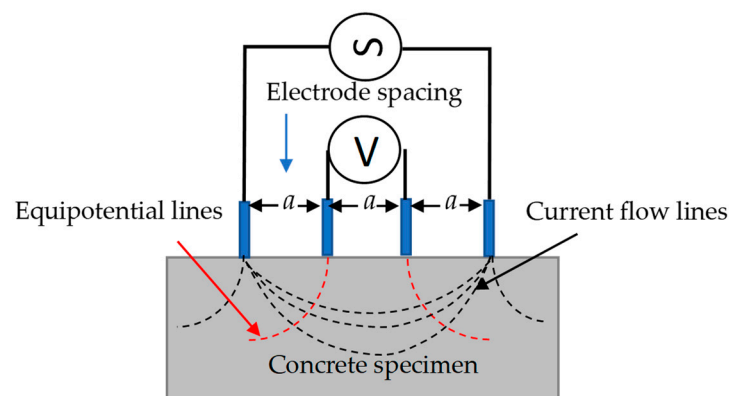


Figure 3. Illustration of the four-point Wenner array to measure surface electrical resistivity.

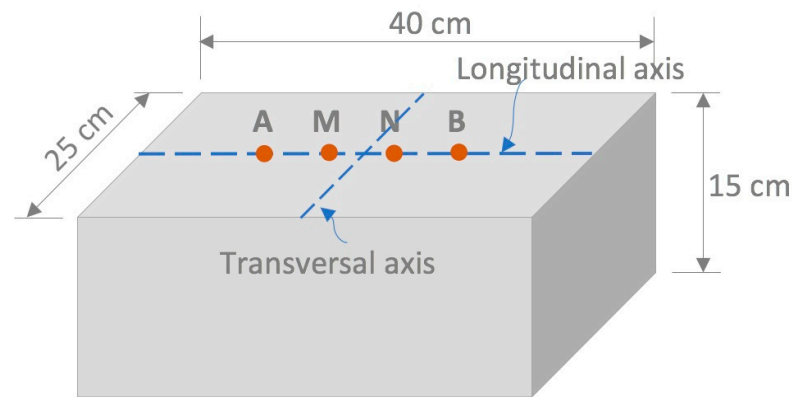


Figure 4. Diagram of the location of the reference axes used in electrical resistivity measurements as a function of electrode separation a . A, M, N, and B are the electrode positions in the specimen.

Three readings were taken for each electrode separation, and the mean and standard deviation were obtained. The electrical resistivity was calculated according to Equation (1), assuming a semi-infinite, homogeneous, and isotropic volume [13,14]:

$$\rho = 2\pi aR \quad (1)$$

where R is the electrical resistance, ρ is the apparent electrical resistivity, and a is the electrode separation of the Wenner array.

AASHTO T358 [19] requires correction of the resistance values based on curing in a saturated calcium hydroxide solution, which was carried out using Equation (2):

$$\rho_{corrected} = \rho k_{LW} \quad (2)$$

where $\rho_{corrected}$ is the true resistivity and k_{LW} is a correction factor for curing the sample in a saturated calcium hydroxide solution ($k_{LW} = 1.1$).

2.2.3. Data Inversion Using the RES1D Free Software

Using the RES1D free software [33], the thickness of two layers with different electrical properties (with and without chlorides) was determined. The program read a data file that contained information such as the estimate of the thickness of the surface layer, at least five data pairs of the electrode separation and their corresponding apparent resistivities (a, ρ), the number of layers sought, their resistivity (ρ), and their thickness (z). To reduce the difference between the observed and calculated values, the model and optimization subroutine modified layer thickness and resistivity were compared. The result of the data inversion represented the depth of the two layers described above.

The initial first layer thickness (penetration depth) values required for the inversion process were estimated with the solution according to Fick's second law of diffusion. The penetration depths were calculated at approximately a 0.0% chloride concentration, assuming a surface concentration of $C_s = 1\%$. The diffusion coefficients were obtained using Equations (3)–(6) [34–36] based on a reference diffusion coefficient that considers the type of binder and w/b ratio:

$$D(t) = D_{ref} (t_{ref}/t)^m \quad (3)$$

where $D(t)$ is the diffusion coefficient (m^2/s) at time t ; D_{ref} is the diffusion coefficient (m^2/s) at reference time t_{ref} ; and m is a constant that depends on the type and amount of binder [37].

$$D_{28} = 10^{(-12.06+2.4w/b)} \quad (4)$$

$$m = 2.5 (w/b)^{-0.6} \quad (5)$$

$$m = 0.2 + 0.4 (\% \text{ FA}/50) \quad (6)$$

where D_{28} is the reference diffusion coefficient (m^2/s); w/b is the water/binder ratio; and % FA is the percentage substitution of Portland cement with fly ash in the mix [35,38].

According to Polder et al. [39] and Cosoli et al. [16], the thickness of the second layer was $z \approx a$ because the resistivity measured with the Wenner configuration is considered as the average of a hemisphere of radius equal to the electrode spacing a , as long as the hypothesis that the medium is homogeneous and semi-infinite is valid.

2.2.4. Chloride Penetration Depth Using the Colorimetric Technique

The specimens were fractured along their longitudinal axis, which coincided with the axis of the electrical resistivity measurements. To conduct the colorimetric test, a freshly fractured sample was sprayed with a 0.1 N silver nitrate (AgNO_3) solution [40]. Silver chloride precipitated, creating a whitish region due to the rapid chemical reaction between the free chlorides and silver nitrate. This color change shows the depth of chloride penetration. The color change prevailed with time, and it was observed that the depth increased if it was measured several hours later. For this reason, measurements were taken every 10 mm with a Vernier caliper, first after spraying AgNO_3 and then 24 h later.

2.2.5. Chloride Content Profiles

Once the specimens used for the colorimetric tests were fractured at 7, 28, 112, and 175 days, a PF-1100 profile grinder (Germann Instruments, Evanston, IL, USA) was used to extract powder samples in 2 mm thick layers (5–7 g per layer). Finally, the powder was processed to determine the acid-soluble chloride ion content via potentiometric titration.

3. Results and Discussion

3.1. Electrical Resistivity Measurements

Figure 5 presents the electrical resistivity data versus electrode spacing in radar-type graphs for specimens that underwent (a) 28 and (b) 220 days of moist curing. The graphs show variations in the electrical resistivity of the specimens as Cl^- diffused, which resulted from the exposure time, electrode separation, w/b ratio, and the type of cementitious materials. In all cases, the percentage variations in resistivity with respect to the zero day of chloride exposure (considered as the control) were calculated.

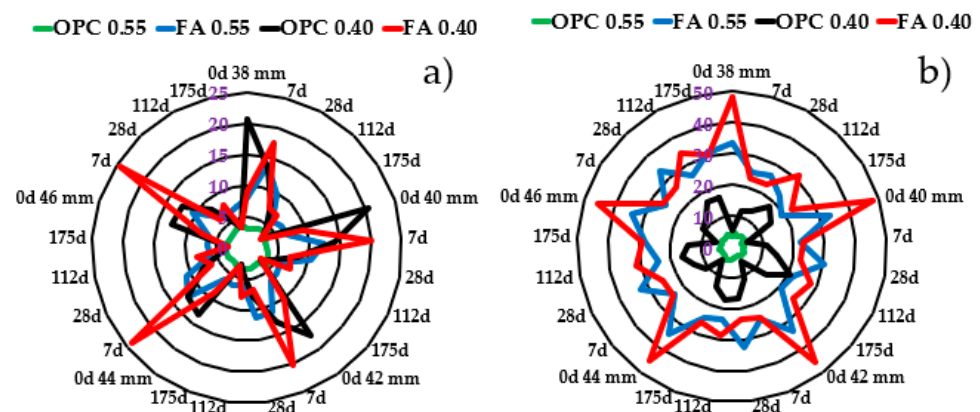


Figure 5. Electrical resistivity in mortar specimens with (a) 28 and (b) 220 days of moist curing at different Cl^- exposure times as a function of electrode spacing: 38, 40, 42, 44, and 46 mm.

When the separation of electrodes was 38 mm, it was observed that the resistivity of OPC0.55 at zero days was the lowest ($3.1 \text{ k}\Omega\cdot\text{cm}$) compared with the other three mortars; although, by test day 175, it increased by approximately 39% of its initial value. A different behavior was exhibited by the OPC0.40, which showed the highest initial resistivity of

20.8 k Ω ·cm and decreased by 35.4% at seven days. At 175 days, the resistivity decreased by 85.9%. For the FA0.55 mortar, the resistivity started at 8 k Ω ·cm, increased by 73% at seven days, and then gradually decreased until it reached 18% below its initial value at 175 days. A similar behavior was exhibited by the FA0.40, which started at 9.1 k Ω ·cm and increased by 91% at seven days, and then gradually decreased until it reached 72% below its initial value. Increasing the electrode separation to 40 mm caused the resistivity to decrease by approximately 5%.

A similar behavior between zero and seven days has been described by Wang et al. [41], who observed that the resistivity does not decrease instantaneously with the ingress of Cl⁻ because there is no contribution to the electric current flow at the moment of chloride ion binding to the hydration products. Similarly, Loche et al. [42] reported that Cl⁻ ions modified the electrical response of cement-based materials. As the Cl⁻ ions penetrated, the electrical resistance initially increased and then decreased, which is in agreement with the behavior of specimens FA0.55 and FA0.40, which were moist-cured for 28 days. As electrical resistivity depends on the chemical composition of the pore solution, the presence of other ions, such as K⁺, Na⁺, OH⁻, and, to a lesser extent, Ca²⁺ and SO²⁻, could affect the resistivity measurements [43]. On the other hand, Minagawa et al. [30] found that electric current flow increases in the region of lower electrical resistivity, and Oleiwi et al. [18] observed that as the Cl⁻ content in the pore solution increases, the resistivity decreases. The latter is in agreement with the findings of Polder et al. [22] and Cosoli et al. [16], who consider the decrease in resistivity to be related to the presence of chloride ions.

Increased electrode spacing allowed deeper probing into the sample [21,31]; for example, by changing *a* from 38 mm to 46 mm, the fraction of the analyzed volume that had electrical properties of the “layer” containing chloride ions decreased and the measurements better reflected the properties of the zone that was free from these ions. Using this strategy, the current flow in the mortar is more homogeneous and the variability in the measurements is lower [22]. The resistivity also decreased as the *w/b* ratio increased, as expected, because of a larger porosity and connectivity.

In contrast to the mortar specimens that were moist-cured for 28 days, where the benefits of using fly ash were marginal, the resistivity of mortars with long moist curing showed a completely different behavior. Figure 5b shows that sample OPC0.55 had the lowest resistivity, with similar values and behavior to the sample that was moist-cured for 28 days. The resistivity started at 3.4 k Ω ·cm and remained nearly constant during the chloride exposure time (175 days). Sample OPC0.40 showed the effects of a lower *w/b* ratio. Its resistivity started at 5.6 k Ω ·cm and increased 2.16 times at seven days, then gradually increased until reaching 2.64 times its initial value at 175 days. For sample FA0.55, the initial resistivity value was much higher (33.8 k Ω ·cm) than samples containing only cement. Its resistivity decreased by 26% in seven days and continued decreasing by up to 44% of its initial value. A similar behavior was observed for sample FA0.40, which started at a resistivity of 48.3 k Ω ·cm and decreased by 53% at seven days; then, it increased at 112 days and decreased again at a resistivity value similar to the one measured at seven days. Increasing the electrode separation (40–46 mm) caused a decrease in the resistivity (by approximately 9%). There was also a decrease in resistivity as the *w/b* ratio increased, as expected.

Specimens that were moist-cured for 28 days had a lower surface resistivity than those cured for 220 days due to the significant cement hydration effects at the early stages, with resistivities ranging from 3 to 20 k Ω ·cm. In contrast, at the longest curing time, the resistivity ranged from 3 to approximately 50 k Ω ·cm (ρ OPC0.55 < ρ OPC0.40 < ρ FA0.55 < ρ FA0.40) due to the denser microstructure and higher degree of hydration. Specimens with a higher *w/b* ratio showed lower resistivity than those with a lower *w/b* ratio. Moreover, specimens with FA had higher resistivity than those constructed only with OPC. This is because of the pozzolanic reaction of FA that produced more C-S-H, thus decreasing the porosity and refining the pore structure. The formation of solid phases such as Friedel’s salt may affect the resistivity.

3.1.1. Electrical Resistivity of Chloride-Free Specimens

Figure 6 shows the resistivity evolution as a function of age, w/b ratio, type of cementitious materials, and specimen geometry. Measurements were performed at 0, 28, 112, and 175 days. The age of the specimens was obtained from the sum of the 28 days of moist curing plus the testing day. As expected, due to hydration reactions, resistivity increased with age in most of the specimens, especially in those containing FA. According to Grazia et al. [44], FA and other SCMs impact concrete's microstructure and pore solution chemistry (alkalinity reduction). They found that the resistivity may increase by up to ten times when adding SCM due to the formation of additional C-S-H, which acts as an electrical barrier. The pozzolanic reaction leads to the partial consumption of portlandite from the system and a decrease in pH. According to Medeiros and Lima [45] and Kang et al. [46], blended cements have higher resistivity than OPC. Although class F FA slows down the C-S-H formation, in the present study, the resistivity was still improved compared with OPC mortars. Reducing the w/b ratio from 0.55 to 0.40 also causes an increase in resistivity due to a reduced porosity and connectivity of lower w/b ratio mortars. Hou [47] observed that the microstructure of the C(A)SH gel conducts water molecules and ions less easily due to the addition of Al^{3+} .

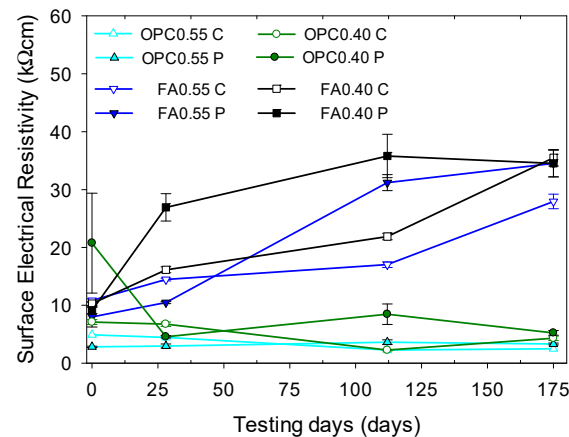


Figure 6. Evolution of electrical resistivity (using $a = 38$ mm) in control prismatic and cylindrical specimens after 28 days of moist curing. Error bars represent \pm one standard deviation.

The shape and size of the specimens had a significant influence on the resistivity, and in all cases, cylindrical specimens showed lower values than prismatic ones. The dispersion of the measured resistivity, expressed by the standard deviation bars, was smaller for cylinders than for prisms due to the propagation geometry of electric waves [48,49]. This is in agreement with the investigations of Hornáková and Lehner [50], who determined that the variance in measured resistivity values in concrete specimens, shown through standard deviation, was two to three times lower for cylindrical geometry than for prismatic geometry.

3.1.2. Electrical Resistivity of Mortars without Hydration Effects Exposed to Chlorides

Figure 7 compares the resistivity of cylindrical and prismatic specimens after 220 days of moist curing that were then subjected to chloride ion diffusion. The effect of hydration on the resistivity of these specimens was expected to be negligible because of the long moist-curing time. As chloride ions diffused into the samples, the resistivities exhibited a distinct behavior depending on the mix composition (mortars containing FA or only OPC), type of specimen, and w/b ratio. Mortars containing only OPC exhibited the lowest resistivities, as mentioned in Section 3.1. The resistivity of the OPC0.55 specimens remained nearly constant during the 175 days. Specimens of OPC0.40 mortar with prismatic geometry demonstrated a twofold increase at seven days; then, the resistivities remained nearly constant. Contrary to this behavior, the cylinders showed a constant resistivity up to 28 days, and then it slightly increased at 112 and 175 days.

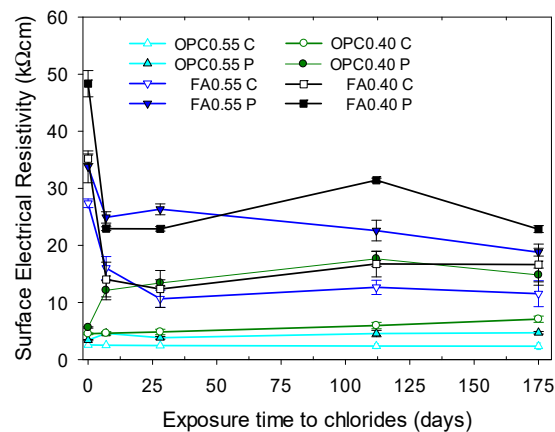


Figure 7. Electrical resistivity of cylindrical (C) and prismatic (P) specimens as a function of exposure time to a 2.8 M NaCl solution, using $a = 38$ mm. The specimens were previously moist-cured in a saturated calcium hydroxide solution for 220 days. Error bars represent \pm one standard deviation.

Mortars containing FA exhibited a different behavior. After seven days, the resistivity of the FA0.55 specimens decreased by around 50% and then continued to decrease gradually. The resistivity of the FA0.40 specimens also significantly decreased at seven days (by approximately 53%), but then it remained nearly constant or slightly increased at 112 and 175 days. As was shown in the previous section (Section 3.1.1), cylindrical specimens had a lower resistivity than prismatic specimens.

3.2. Chloride Penetration Depth Using Three Different Techniques

Figure 8 illustrates the chloride penetration depth measured in the mortar specimens immediately after spraying silver chloride on the fractured surface. As expected, the penetration depth increased with chloride exposure time. At the end of the exposure to chlorides (175 days), the highest penetration was observed for the OPC0.55 mortar, followed by OPC0.40. The lowest penetration depth was seen for FA0.55, and FA0.40 had the highest resistivity. The chloride concentration for color change depends on the amount of OH^- ions in the pore solution. This ranges from 0.28 to 1.69% by mass of cement or between 0.072 and 0.714 mol/L for the AgNO_3 technique [51]. In addition, there is no consensus on the chloride concentration corresponding to the color change boundary. The average level of soluble Cl^- detected at the color change boundary was 0.9 wt.% cementitious materials or 0.12 wt.% concrete, with high coefficients of variation of 33% and 40%, respectively [40]. The amount of AgCl and Ag_2O formed at the color change boundary depends on the Cl^-/OH^- ratio in the pore solution and can be seen as an estimation of the chloride ion penetration depth, rather than the actual boundary between chloride-containing and chloride-free areas.

When performing the colorimetric test, the presence of a diffuse zone was detected between the zone with and without chlorides, which was difficult to measure immediately after spraying with AgNO_3 . Therefore, the decision was made to keep the samples under the laboratory conditions, and a second measurement was performed 24 h later. The second measurement showed a higher chloride penetration depth than that observed immediately after spraying. Figure 9 shows photographs from two specimens at 0 and 24 h after spraying. The white region depth increased by an average of 27% at 24 h after spraying the AgNO_3 solution. To the best of our knowledge, this observation has not been reported in the existing literature.

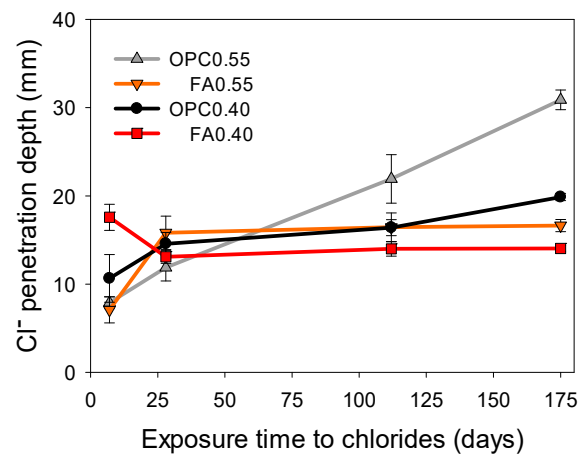


Figure 8. Chloride penetration depth versus the exposure time from AgNO_3 solution spraying.

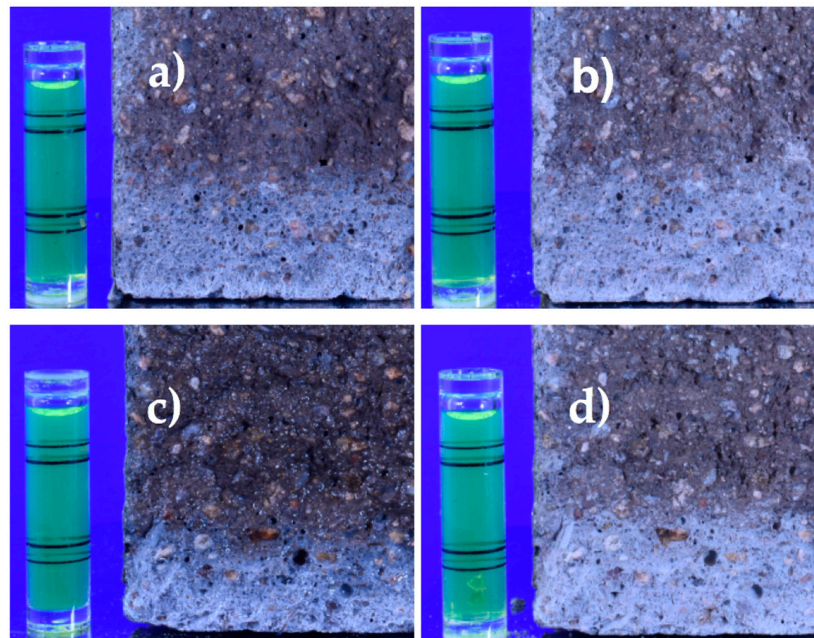


Figure 9. Change in penetration depth with time in the colorimetric test: (a) OPC0.55 at 0 h, (b) OPC0.55 at 24 h, (c) FA0.55 at 0 h, and (d) FA0.55 at 24 h after spraying the AgNO_3 on the broken surface. The bubble level was 40 mm in height.

SCMs change how the hydrated cement paste phases are formed, and thus, their Cl^- binding properties [52]. For example, FA is a material rich in reactive aluminates and exhibits increased AFm formation and, therefore, increased Cl^- binding in the C(A)SH. A decrease in the amount of Ca^{2+} causes a decrease in the amount of Cl^- bound to AFm and an increase in the amount bound to C(A)SH since it is a portlandite-deficient system. The ingress of Cl^- reduces the adsorption of Al^{3+} from C(A)SH and increases the amount of Al^{3+} available to form chloride-bound AFm.

In the present study, a 2.8 M NaCl concentration was used; therefore, the Cl^- ions entering the system must compete to displace the SO_4^{2-} , OH^- , and/or CO_3^{2-} anions of the different monosulfoaluminates and, finally, Friedel salt is formed [4]. According to Balonis et al. [4], at high chloride concentrations the Kuzel salt or monocarboaluminate phases are destabilized by increasing the chemically bound chloride so that a high chloride concentration would make the formation of the AFm phases, such as the Kuzel salt, impossible. When the systems destabilize, ions such as sulfate ions can be released, and

they react with calcium and aluminum, forming ettringite and causing expansion due to the increase in the molar volume of the solid and refining of the porosity [4].

Figure 10 shows the chloride content profiles for the mortar specimens obtained via potentiometric titration, as well as the chloride penetration depth obtained by spraying the AgNO_3 solution. Figure 10a shows that OPC0.55 had the highest Cl^- penetration, reaching a depth of approximately 38 mm at 175 days of chloride diffusion, whereas for FA0.55, the depth reached 22 mm (Figure 10b). The latter was expected because of the presence of FA. In the same manner, OPC0.40 (Figure 10c) had a 26 mm penetration, and FA0.40 (Figure 10d) exhibited the lowest penetration (18 mm). The measurements were taken at the color change boundary immediately after spraying the freshly fractured surfaces with the AgNO_3 solution. This test underestimates the chloride penetration depth.

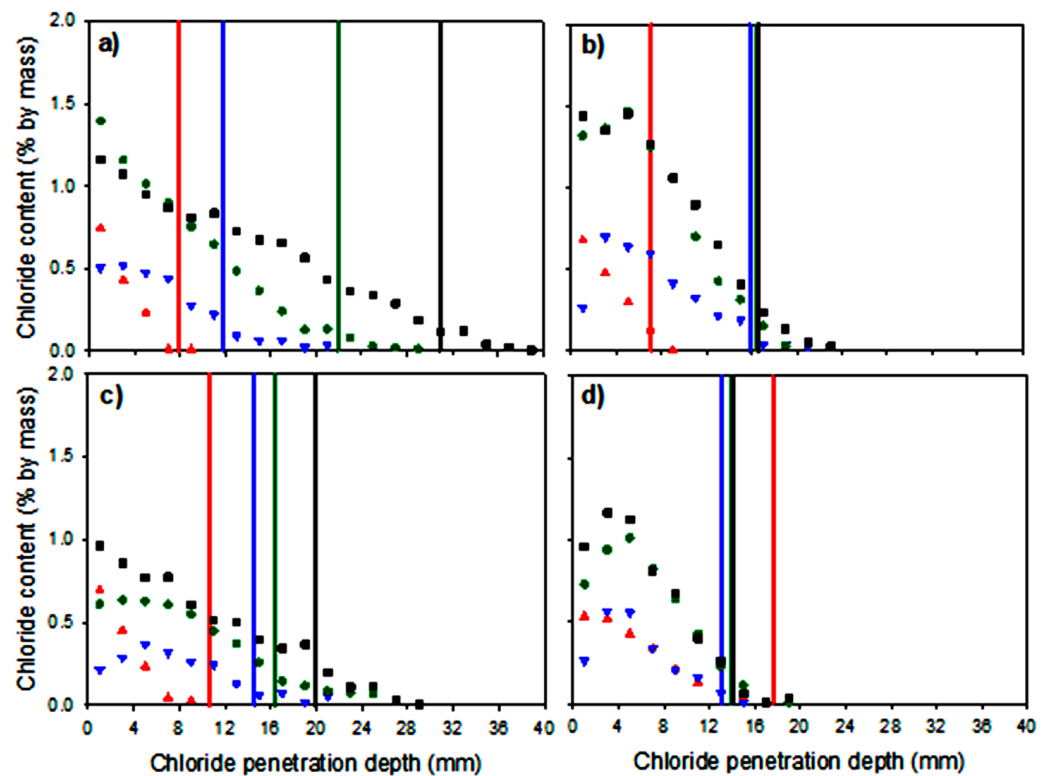


Figure 10. Total chloride content profiles and chloride penetration depth determined using colorimetry after spraying and at 7 (red), 28 (blue), 112 (green), and 175 (black) days of exposure to chlorides: (a) OPC0.55, (b) FA0.55, (c) OPC0.40, and (d) FA0.40.

Table 4 presents the apparent diffusion coefficients calculated by fitting the data of the chloride content profiles shown in Figure 10 to the solution of Fick's second law of diffusion [34]. The trends observed in the diffusion coefficient from 28 days up to 175 days of exposure to chlorides show higher values for the high w/b ratios and lower values for the low w/b ratios, as expected. Moreover, the mortars containing fly ash exhibited lower diffusion coefficients than the mortars containing only OPC because of the pozzolanic reaction that produces additional C-S-H and reduces porosity and permeability.

A linear relationship between the penetration depths from spraying the AgNO_3 solution and the concentration profiles is shown in Figure 11. There is a linear correlation ($R^2 = 0.96$) between them with a slope < 1 , indicating an underestimation with the colorimetric method.

Table 4. The apparent diffusion coefficient and surface chloride concentration of mortar specimens moist-cured for 28 days determined by fitting chloride content profiles to the solution of Fick’s second law of diffusion [34].

Exposure Time (Days)	OPC0.55		FA0.55		OPC0.40		FA0.40	
	D (m ² /s)	C _s (%)						
7	2.6 × 10 ⁻¹¹	1.09	4.1 × 10 ⁻¹¹	0.98	3.3 × 10 ⁻¹¹	1.00	1.2 × 10 ⁻¹⁰	1.85
28	6.8 × 10 ⁻¹¹	0.79	5.0 × 10 ⁻¹¹	1.08	7.0 × 10 ⁻¹¹	0.70	2.9 × 10 ⁻¹¹	0.96
112	1.4 × 10 ⁻¹¹	1.62	5.6 × 10 ⁻¹²	3.00	1.8 × 10 ⁻¹¹	1.04	5.0 × 10 ⁻¹²	2.12
175	2.6 × 10 ⁻¹¹	1.41	5.6 × 10 ⁻¹²	2.46	1.4 × 10 ⁻¹¹	1.00	4.0 × 10 ⁻¹²	1.85

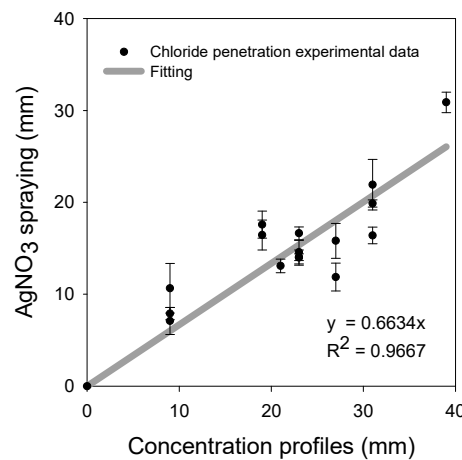


Figure 11. Relationship between the penetration depth of Cl⁻ in mortar specimens at different days of chloride exposure obtained using colorimetry after spraying a 0.1 N AgNO₃ solution, and the distance from concentration profiles. Error bars represent ± one standard deviation.

Another alternative way of obtaining the depth of chloride penetration proposed in this study is by inverting the surface electrical resistivity data obtained at different exposure times to 2.8 M NaCl. Figure 12 shows that, as expected, for mortars with high *w/b* ratios or the case of fly-ash-free mixtures, the chloride penetration was higher.

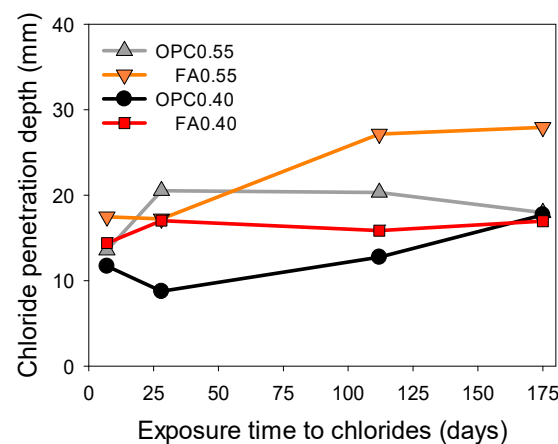


Figure 12. Chloride penetration depth in mortar specimens OPC0.55, FA0.55, OPC0.40, and FA0.40 obtained via inversion of resistivity data at different exposure times to 2.8 M NaCl solution.

Figure 13 shows two linear correlations of the chloride penetration depth determined through inversion of the resistivity data at different Cl⁻ exposure times. The first of these is R² = 0.86, determined by comparing it with the depth of chloride ion penetration obtained

via the colorimetric method, while the second is $R^2 = 0.86$, determined by comparing it with the depth of chloride ion penetration determined via the chloride content profiles. The first correlation indicates that the resistivity measurements are underestimates and the second one overestimates the chloride penetration. Fares et al. [25] obtained chloride profiles using electrical resistivity tomography (ERT) and compared them with those obtained using the chloride content of powder samples. They observed a good agreement between ERT and the destructive test because they used a smaller electrode separation than in our study, which was restricted to a minimum of 38 mm. In addition, their electrodes maintained a fixed relative position to perform the measurement with all electrode separations, which resulted in a lower variability of measurements.

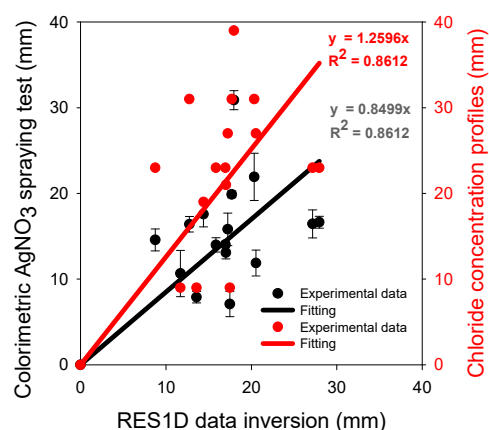


Figure 13. Correlation between Cl^- penetration depth obtained via resistivity data inversion and that obtained using the colorimetric test and chloride content profiles on mortar specimens on different days of chloride exposure. Error bars represent \pm one standard deviation.

4. Conclusions

This study explored the use of a simple Wenner array to measure changes in the surface electrical resistivity of mortars subject to chloride diffusion under laboratory conditions as a function of electrode separation. The following conclusion is given: Diffusion of chlorides in mortar specimens affects the resistivity measured with a simple Wenner array with variable electrode separation after inversion with the RES1D software, which permits indirect calculation of the chloride penetration depth. This was validated through a linear correlation with AgNO_3 spraying and chloride concentration profiling, both resulting in an R^2 of approximately 0.86.

Author Contributions: Conceptualization, M.A.P.-C. and P.F.d.J.C.-B.; formal analysis, M.A.P.-C., P.F.d.J.C.-B. and F.M.L.-M.; funding acquisition, P.F.d.J.C.-B.; investigation, M.A.P.-C. and F.M.L.-M.; methodology, M.A.P.-C. and P.F.d.J.C.-B.; project administration, P.F.d.J.C.-B.; supervision, P.F.d.J.C.-B.; writing—original draft, M.A.P.-C.; writing—review and editing, P.F.d.J.C.-B. and F.M.L.-M. All authors have read and agreed to the published version of the manuscript.

Funding: This research was funded by SIP of Instituto Politécnico Nacional under grant numbers SIP 20210481, SIP 20221260, and SIP 20231520. The APC was funded by project SIP 20231520.

Institutional Review Board Statement: Not applicable.

Informed Consent Statement: Not applicable.

Data Availability Statement: The data presented in this study are available on request from the corresponding author.

Acknowledgments: M. Pablo-Calderón acknowledges CONACYT (now CONAHCYT) from Mexico for the Graduate Studies scholarship, COFAA-IPN for an Institutional Scholarship for Researcher Training (BEIFI), and the IPN program “Technological Development and Innovation Projects” for IPN Students 2022 for funding this project. P. Cano acknowledges SIP from IPN for funding the research projects with ID codes SIP 20210481, SIP 20221260, and SIP 20231520. The authors acknowledge Erick León Pérez for providing the photos shown in Figure 8.

Conflicts of Interest: The authors declare no conflict of interest.

References

1. Neville, A. Chloride Attack of Reinforced Concrete: An Overview. *Mater. Struct.* **1995**, *28*, 63–70. [[CrossRef](#)]
2. Spragg, R.; Bu, Y.; Snyder, K.; Bentz, D.; Weiss, J. *Electrical Testing of Cement-Based Materials: Role of Testing Techniques, Sample Conditioning, and Accelerated Curing*; Indiana Department of Transportation and Purdue University: West Lafayette, IN, USA, 2013.
3. Spragg, R.; Villani, C.; Snyder, K.; Bentz, D.; Bullard, J.; Weiss, J. Factors That Influence Electrical Resistivity Measurements in Cementitious Systems. *Transp. Res. Rec. J. Transp. Res. Board* **2013**, *2342*, 90–98. [[CrossRef](#)]
4. Balonis, M.; Lothenbach, B.; Le Saout, G.; Glasser, F.P. Impact of Chloride on the Mineralogy of Hydrated Portland Cement Systems. *Cem. Concr. Res.* **2010**, *40*, 1009–1022. [[CrossRef](#)]
5. Marvila, M.T.; de Azevedo, A.R.G.; Ferreira, R.L.S.; Vieira, C.M.F.; de Brito, J.; Adesina, A. Validation of Alternative Methodologies by Using Capillarity in the Determination of Porosity Parameters of Cement-Lime Mortars. *Mater. Struct. Constr.* **2022**, *55*, 19. [[CrossRef](#)]
6. Coates, G.R.; Xiao, L.; Prammer, M.G. *NMR Logging Principles and Applications*; Halliburton Energy Services: Houston, TX, USA, 1999; ISBN 9780080438801.
7. *ASTM C1202*; Standard Test Method for Electrical Indication of Concrete’s Ability to Resist Chloride Ion Penetration. ASTM International: West Conshohocken, PA, USA, 2012.
8. *NT BUILD 492*; Concrete, Mortar and Cement-Based Repair Materials: Chloride Migration Coefficient from Non-Steady-State Migration Experiments. NORDTEST: Espoo, Finland, 1999.
9. *AASHTO T259*; Standard Method of Test for Resistance of Concrete to Chloride Ion Penetration. American Association of State Highway and Transportation Officials: Washington, DC, USA, 2009.
10. *NT BUILD 443*; Concrete, Hardened: Accelerated Chloride Penetration. NORDTEST: Espoo, Finland, 2010.
11. *ASTM C1556*; Standard Test Method for Determining the Apparent Chloride Diffusion Coefficient of Cementitious Mixtures by Bulk Diffusion. ASTM International: West Conshohocken, PA, USA, 2003.
12. Jenkins, A. *Surface Resistivity as an Alternative for Rapid Chloride Permeability Test of Hardened Concrete (FHWA-KS-14-15)*; Kansas Department of Transportation Bureau of Research: Kansas City, MO, USA, 2015.
13. *ASTM C1876-19*; Standard Test Method for Electrical Resistivity or Conductivity of Concrete. ASTM International: West Conshohocken, PA, USA, 2019.
14. *AASHTO TP 119*; Standard Method of Test for Electrical Resistivity of a Concrete Cylinder Tested in a Uniaxial Resistance Test. American Association of State Highway and Transportation Officials: Washington, DC, USA, 2017.
15. Morris, W.; Moreno, E.I.; Sagués, A.A. Practical Evaluation of Resistivity of Concrete in Test Cylinders Using a Wenner Array Probe. *Cem. Concr. Res.* **1996**, *551*–556. [[CrossRef](#)]
16. Cosoli, G.; Mobili, A.; Tittarelli, F.; Revel, G.; Chiariotti, P. Electrical Resistivity and Electrical Impedance Measurement in Mortar and Concrete Elements: A Systematic Review. *Appl. Sci.* **2020**, *10*, 9152. [[CrossRef](#)]
17. Millard, S.G. Reinforced Concrete Resistivity Measurement Techniques. *Proc.-Inst. Civ. Eng. Part 2 Res. Theory* **1991**, *91*, 71–88. [[CrossRef](#)]
18. Oleiwi, H.; Wang, Y.; Xiang, N.; Chen, X.; Shabalin, I. An Experimental Study of Concrete Resistivity and the Effects of Electrode Configuration and Current Frequency on Measurement. In Proceedings of the Sixth International Conference on Durability of Concrete Structures, Leeds, UK, 18–20 July 2018; pp. 592–599.
19. *AASHTO T358-15*; Standard Method of Test for Surface Resistivity Indication of Concrete’s Ability to Resist Chloride Ion Penetration. American Association of State Highway and Transportation Officials: Washington, DC, USA, 2015.
20. Cheytani, M.; Chan, S.L.I. The Applicability of the Wenner Method for Resistivity Measurement of Concrete in Atmospheric Conditions. *Case Stud. Constr. Mater.* **2021**, *15*, e00663. [[CrossRef](#)]
21. Robles, K.P.V.; Yee, J.J.; Kee, S.H. Effect of the Geometrical Constraints to the Wenner Four-Point Electrical Resistivity Test of Reinforced Concrete Slabs. *Sensors* **2021**, *21*, 4622. [[CrossRef](#)]
22. Polder, R.B. Test Methods for on Site Measurement of Resistivity of Concrete—A RILEM TC-154 Technical Recommendation. *Constr. Build. Mater.* **2001**, *15*, 125–131. [[CrossRef](#)]
23. Qiao, C.; Moradillo, M.K.; Hall, H.; Tyler Ley, M.; Weiss, W.J. Electrical Resistivity and Formation Factor of Air-Entrained Concrete. *ACI Mater. J.* **2019**, *116*, 85–93. [[CrossRef](#)]
24. Layssi, H.; Ghods, P.; Alizadeh, A.; Salehi, M. Electrical Resistivity of Concrete. *Concr. Int.* **2015**, *37*, 41–46.
25. Fares, M.; Villain, G.; Bonnet, S.; Palma Lopes, S.; Thauvin, B.; Thiery, M. Determining Chloride Content Profiles in Concrete Using an Electrical Resistivity Tomography Device. *Cem. Concr. Compos.* **2018**, *94*, 315–326. [[CrossRef](#)]

26. ASTM C128-01; Standard Test Method for Density, Relative Density (Specific Gravity), and Absorption. ASTM International: West Conshohocken, PA, USA, 2001.
27. Ramírez Ortiz, A.E. Respuesta Ultrasónica de Pastas de Cemento Sujetas a Difusión y Ligado de Iones Cloruro. Ph.D. Thesis, Instituto Politécnico Nacional, Ciudad de México, Mexico, 2018.
28. ASTM C192/C192M; Standard Practice for Making and Curing Concrete Test Specimens in the Laboratory. ASTM International: West Conshohocken, PA, USA, 2002.
29. ASTM C109/C109M-02; Standard Test Method for Compressive Strength of Hydraulic Cement Mortars. ASTM International: West Conshohocken, PA, USA, 2002.
30. Minagawa, H.; Miyamoio, S.; Hisada, M. Relationship of Apparent Electrical Resistivity Measured by Four Probe Method with Water Content Distribution in Concrete. *J. Adv. Concr. Technol.* **2017**, *15*, 278–289. [[CrossRef](#)]
31. Gowers, K.R.; Millard, S.G. Measurement of Concrete Resistivity for Assessment of Corrosion Severity of Steel Using Wenner Technique. *ACI Mater. J.* **1999**, *96*, 536–541. [[CrossRef](#)]
32. Chen, C.T.; Chang, J.J.; Yeih, W.C. The Effects of Specimen Parameters on the Resistivity of Concrete. *Constr. Build. Mater.* **2014**, *71*, 35–43. [[CrossRef](#)]
33. Loke, M. 1-D Resistivity, IP & SIP Inversion and Forward Modeling Wenner and Schlumberger Arrays. Available online: <https://www.geotomosoft.com/downloads.php> (accessed on 20 June 2019).
34. Nokken, M.; Boddy, A.; Hooton, R.D.; Thomas, M.D.A. Time Dependent Diffusion in Concrete-Three Laboratory Studies. *Cem. Concr. Res.* **2006**, *36*, 200–207. [[CrossRef](#)]
35. Bentz, E.C.; Thomas, M. Life-365 Service Life Prediction Model and Computer Program for Predicting the Service Life and Life-Cycle Cost of Reinforced Concrete Exposed to Chlorides. Available online: <http://www.life-365.org/download.html> (accessed on 15 January 2019).
36. Villagrán-Zaccardi, Y.A. Ingreso de Cloruro En Hormigones Con Cemento Pórtland Compuesto. Influencias Del Tiempo y de La Capacidad de Fijación. Ph.D. Thesis, Universidad Nacional del Centro de la Provincia de Buenos Aires, Tandil, Argentina, 2009.
37. Mangat, P.S.; Molloy, B.T. Prediction of Long Term Chloride Concentration in Concrete. *Mater. Struct.* **1994**, *27M*, 338–346. [[CrossRef](#)]
38. Park, K.B.; Lee, H.S.; Wang, X.Y. Prediction of Time-Dependent Chloride Diffusion Coefficients for Slag-Blended Concrete. *Adv. Mater. Sci. Eng.* **2017**, *2017*, 1901459. [[CrossRef](#)]
39. Polder, R.; Andrade, C.; Elsener, B.; Vennesland, Ø.; Gulikers, J.; Weidert, R.; Raupach, M. RILEM TC 154-EMC: Electrochemical Techniques for Measuring Metallic Corrosion. Test Methods for on Site Measurement of Resistivity of Concrete. *Mater. Struct.* **2000**, *33*, 603–611.
40. Meck, E.; Sirivivatnanon, V. Field Indicator of Chloride Penetration Depth. *Cem. Concr. Res.* **2003**, *33*, 1113–1117. [[CrossRef](#)]
41. Wang, Y.; Nanukuttan, S.; Bai, Y.; Yang, K.; Basheer, M. Electrical Resistance to Monitor Carbonation and Chloride Ingress. *ACI Mater. J.* **2019**, *116*, 129–138. [[CrossRef](#)]
42. Loche, J.M.; Ammar, A.; Dumargue, P. Influence of the Migration of Chloride Ions on the Electrochemical Impedance Spectroscopy of Mortar Paste. *Cem. Concr. Res.* **2005**, *35*, 1797–1803. [[CrossRef](#)]
43. Tibbetts, C.M.; Paris, J.M.; Ferraro, C.C.; Riding, K.A.; Townsend, T.G. Relating Water Permeability to Electrical Resistivity and Chloride Penetrability of Concrete Containing Different Supplementary Cementitious Different Supplementary Cementitious Materials. *Cem. Concr. Compos.* **2020**, *107*, 103491. [[CrossRef](#)]
44. de Grazia, M.T.; Deda, H.; Sanchez, L.F.M. The Influence of the Binder Type & Aggregate Nature on the Electrical Resistivity of Conventional Concrete. *J. Build. Eng.* **2021**, *43*, 102540. [[CrossRef](#)]
45. Medeiros, R.A.; Lima, M.G. Electrical Resistivity of Unsaturated Concrete Using Different Types of Cement. *Constr. Build. Mater.* **2016**, *107*, 11–16. [[CrossRef](#)]
46. Kang, S.; Tyler Ley, M.; Lloyd, Z.; Kim, T. Using the Particle Model to Predict Electrical Resistivity Performance of Fly Ash in Concrete. *Constr. Build. Mater.* **2020**, *261*, 119975. [[CrossRef](#)]
47. Hou, D.; Li, T.; Wang, P. Molecular Dynamics Study on the Structure and Dynamics of NaCl Solution Transport in the Nanometer Channel of CASH Gel. *ACS Sustain. Chem. Eng.* **2018**, *6*, 9498–9509. [[CrossRef](#)]
48. du Plooy, R.; Villain, G.; Palma Lopes, S.; Ihamouten, A.; Dérobert, X.; Thauvin, B. Electromagnetic Non-Destructive Evaluation Techniques for the Monitoring of Water and Chloride Ingress into Concrete: A Comparative Study. *Mater. Struct. Constr.* **2015**, *48*, 369–386. [[CrossRef](#)]
49. Samouëlian, A.; Cousin, I.; Tabbagh, A.; Bruand, A.; Richard, G. Electrical Resistivity Survey in Soil Science: A Review. *Soil Tillage Res.* **2005**, *83*, 173–193. [[CrossRef](#)]
50. Horňáková, M.; Lehner, P. Relationship of Surface and Bulk Resistivity in the Case of Mechanically Damaged Fibre Reinforced Red Ceramic Waste Aggregate Concrete. *Materials* **2020**, *23*, 5501. [[CrossRef](#)]

51. He, F.; Shi, C.; Yuan, Q.; Chen, C.; Zheng, K. AgNO₃ Based Colorimetric Methods for Measurement of Chloride Penetration in Concrete. *Constr. Build. Mater.* **2012**, *26*, 1–8. [[CrossRef](#)]
52. De Weerd, K. Chloride Binding in Concrete: Recent Investigations and Recognised Knowledge Gaps: RILEM Robert L’Hermitte Medal Paper 2021. *Mater. Struct.* **2021**, *54*, 1–16. [[CrossRef](#)]

Disclaimer/Publisher’s Note: The statements, opinions and data contained in all publications are solely those of the individual author(s) and contributor(s) and not of MDPI and/or the editor(s). MDPI and/or the editor(s) disclaim responsibility for any injury to people or property resulting from any ideas, methods, instructions or products referred to in the content.